The role of the attrition milling on the grain size and distribution of the carbon nanotubes in YSZ powders

Soukaina Lamnini [a,b], Zsolt Fogarassy [b], Zsolt Endre Horváth [b], Sára Tóth [c], Katalin Balázsi [b,*], Csaba Balázsi [b]

[a] Doctoral School of Material Science and Technologies, Óbuda University, Bécsi str.96/B, 1034 Budapest, Hungary
[b] Institute for Technical Physics and Materials Science, Centre for Energy Research, Hungarian Academy of Sciences, Konkoly – Thege M. str. 29-33, 1121 Budapest, Hungary
[c] Wigner Research Centre for Physics, Hungarian Academy of Sciences, Konkoly – Thege M. str. 29-33, 1121 Budapest, Hungary

ARTICLE INFO

ABSTRACT

The aim of present work was the examination of the role of the high efficient attrition milling on the structure and grain size of $ZrO_2 - 8\,mol.\%\ Y_2O_3$ (YSZ) and on the distribution of multiwall carbon nanotubes (MWCNTs) in these powder mixtures. The microstructure of YSZ/MWCNTs powder mixtures with 1, 5, 10 wt.% MWCNTs was investigated. Detailed study confirmed the YSZ grain size decrease and simultaneously the non-destructive homogenization of MWCNTs in the ceramic powder mixtures. The best homogenization degree was achieved in the case of YSZ/1 wt.% MWCNT powder. Raman scattering measurements were performed to investigate the atomic bonding and structural integrity of carbon nanotubes. The presence of the G and D bands in each samples at ~1590 and $\sim1355\,cm^{-1}$ confirmed the unaffected structural integrity of MWCNTs after the milling process. In addition to Raman measurements the high resolution transmission electron microscopy (HRTEM) studies have shown that the structure of MWCNTs remains intact after milling.

El rol de la molienda por atrición en el tamaño de grano y la distribución de nanotubos de carbono en los polvos YSZ

RESUMEN

El propósito de este trabajo fue la evaluación del rol de la molienda por atrición en la estructura y tamaño de grano de ZrO2 – 8 mol.% Y2O3 (YSZ) y la distribución de tubos de carbono multipared(MWCNTs) en las mencionadas mesclas mixtas pulverizadas. Se investigó la microestructura de los polvos YSZ/MWCNT. El estudio detallado confirmó la disminución del tamaño de grano YSZ y, simultáneamente, la homogeneización no destructiva de

* Corresponding author.
E-mail address: balazsi.katalin@energia.mta.hu (K. Balázsi).

MWCNT en las mezclas cerámicas pulverizadas. El mejor grado de homogenización fue alcanzado en el caso de YSZ al 1% en peso de MWCNT. Se realizaron mediciones de dispersión Raman para investigar la unión atómica y la integridad estructural de los nanotubos de carbono. La presencia de las bandas G y D en cada muestra a ~1590 cm-1 y ~1355 cm-1, confirmó que la integridad estructural de los MWCNT, no fue afectada después del proceso de molienda. Además de las mediciones de Raman, los estudios de microscopía electrónica de transmisión de alta resolución (HRTEM) demostraron que la estructura de los MWCNT permanece intacta después de la molienda.

Introduction

Investigation of advanced ceramics, namely zirconia and their composites became an important task for tremendous scientific research dealing with energy production, conversion and storage. The incorporation of an additive phase into zirconia matrix appears as a very promising approach, especially for enhancing the thermo-mechanical and the electrical properties of the composites [1]. Therefore, advanced ceramics are widely explored for energy applications and different ceramic components are applied to solid oxide fuel cells, super capacitors, hydrogen storage systems and photovoltaic solar cells [2]. Fuel cells are classified according to two different categories. The first one depends on the nature of the fuels used for power generation [3] such as hydrogen [4], methanol [5], fossil fuels [4] or biomass-derived materials [6]. The second category includes the composition of the catalysts to speed up the electrochemical processes regarding the different possible working temperature of the cell [7]. The solid oxide fuel cells (SOFC) operating at high temperature from 800 °C to 1000 °C are one of the best efficient power generation devices devoted to produce clean energy without environmental damages [8]. Yttria-stabilized zirconia (YSZ) is used to be the most frequently electrolyte material for SOFC [9] to convert the chemical energy of the reactants directly into electricity and heat. The output of the reaction is water. The high temperature can cause many problems in terms of anode-electrolyte–cathode degradation and lifetime of the cells [10]. The main challenge is the decrease of the high working temperature of fuel cells. Liu et al. identified and analyzed the main issues responsible for cathode degradation in SOFC [11]. The microstructural changes at the interface of LSM ($(La_xSr_{1-x})_yMnO_3$)/YSZ cathode and YSZ electrolyte introduced a reduction of the LSM craters and the formation of new phases of the insulating zirconate. The lack of oxygen content in the air introduced to the cathode gas was attributed as a major factor responsible of LSM craters reduction. Ni-YSZ cermet anodes are the most common electrode for SOFC operating at high temperature. The metallic Ni particles are responsible of electron conduction produced from hydrogen oxidation according to the following reaction [12]:

$$2H_2 + 2O^{2-} \rightarrow 2H_2O + 4e^- \qquad (1)$$

The high porosity density is recommended for Ni-YSZ cermet anodes to ensure the required performance of the cells.

Indeed, Triple Phase Boundary (TPB) is the point where Ni, YSZ, and the pore meet and participate in electrochemical reaction [13]. The produced water molecule is transferred outside of the anode through the pores. Ni-YSZ anodes work as a catalyst used to reform the methane. Therefore, impurities such as carbon deposition named also "cooking" or "sulphur deposition" remain the major issues responsible for the fast anode deterioration. The presence of sulphur and intensive sulphur deposition contributed to the delamination of anode layer and block the nickel grains. This fact caused the limitation of the hydrogen atom's movement and thus leads to a significant decrease of the cell efficiency. Cheng et al. found that the formation of sulphide (Ni_3S_2, NiS) can be limited by a high cooling rate about 70 °C/min [14]. While the carbon deposition on the porous anode can occur in different forms such as fibres, whiskers or graphitic carbon causing micro morphological changes of the anode resulting in deactivation or breakdown of the catalysts [15]. Many recent studies proved that the temperature of sintering is an important parameter in obtaining a small grained structure for a better performance of SOFC electrolyte [16].

One of the advanced application of ceramics as solar cells resulted in low thermal emittance and increased corrosion resistance at elevated temperatures by applying of the additional layers of zirconium thin film between substrate and absorber [17]. Supercapacitors are developed on the basis of zirconia doped CNT or graphene characterized by enhanced mechanical and electrochemical properties. Amirante et al. concluded that the capacitance of supercapacitor materials is depending strongly on the carbon nanotubes (CNTs) orientation [18]. Alves et al. studied the new concept of a ternary composite consisting of ZrO_2 nanoparticles, reduced graphene oxide (rGO) and in situ polymerized Pyrrole (PPy). It was proved that the addition of zirconia influenced the morphology and increased the porosity of the electrodes resulting in remarkable enhancement in the capacitance of the supercapacitor [19]. On the other hand, a significant improvement in both compressive and torsional resistance has been reported. Different alloys of metal hydrides materials have been studied in the literature namely: cerium, lanthanum and nickel (Ce-La-Ni) or magnesium hydride combined with zirconium oxide and single-walled carbon nanotubes. However, this modern method of storage has some limitations as high thermal stability, difficulty to decompose the hydride system into metal and hydrogen gas or a poor kinetics rate of hydrogenation and dehydrogenation. El-Eskandaranyetal et al. studied the doping effect of MgH_2

nano-powders with 10 wt.% of nanocrystallite $ZrNi_5$ on the hydrogenation/dehydrogenation behaviour [20]. These results showed improved properties with a short absorption time of 1 and 10 min to release 5.3 wt.% of H_2. This study confirmed that the zirconium tetrachloride ($ZrCl_4$) as a catalyst into MgH_2 exhibited a notable reduction in the dehydrogenation and rehydrogenation temperature. More importantly, $ZrCl_4$ prevented the grain growth of the hydride for better cyclic performance [21].

The aim of our study was the development of YSZ/MWCNTs as nickel free SOFC material. This work presents the main results of first preparation step; milling and homogenization. The detailed structural design of milled YSZ/MWCNT powder mixtures with various addition of MWCNTs from 1 to 10 wt.% was performed. The structural and morphological properties of powder mixtures were investigated by scanning electron microscopy (SEM), transmission electron microscopy (TEM), high resolution transmission electron microscopy (HRTEM), X-ray diffraction (XRD) and Raman spectroscopy.

Experimental

Preparation of powder mixtures

ZrO_2 – 8 mol.% Y_2O_3 (yttria-stabilized zirconia (YSZ), Sulzer Metco AMDRY 6643) with an average grain size 40 μm was used as base material for powder mixture preparation (Table 1, Fig. 1a). Commercially available multiwall carbon nanotubes (MWCNT, type NC3100^{TM}, Nanocyl) with an average diameter 9.5 nm and an average length 1.5 μm were added to zirconia

Table 1 – Composition of reference sample and YSZ/MWCNTs powders.

Sample	YSZ (wt.%)	MWCNT (wt.%)
YSZ-100	100	0
YSZ-99	99	1
YSZ-95	95	5
YSZ-90	90	10

powder at different concentrations (1, 5 and 10 wt.%) (Table 1, Fig. 1b, c). High efficiency attritor milling (Union Process, type 01-HD/HDDM) was used (4000 rpm, 5 h) for powder mixture preparation. Each batch with 80 g final product was mixed in zirconia tank (750 cm^3) by 130 g ethanol and 280 mL zirconia balls (each of 1 mm diameter). The obtained powder mixtures were dried at 172 °C for 25 minutes, then sieved by 100 μm mesh (Fig. 1d).

Characterization methods

The phase analysis was performed by X-ray diffractometry (XRD) with Cu Kα radiation using a Bruker AXS D8 Discover diffractometer equipped with Göbel-mirror and a scintillation detector. Energy dispersive X-ray spectroscopy (EDS, Rontec Si (Li) detector with ultrathin window) was used for elemental identification of the powder mixtures after 5 h of milling. The morphology and the characterization of the powders were studied by Scanning Electron Microscopy (SEM, LEO1540 XB) and Transmission Electron Microscopy (TEM, Philips CM-20) and High Resolution Transmission Electron Microscopy (HRTEM, JEOL 3010) operating at 200 and 300 kV, respectively. Raman spectroscopy is a well-known, non-destructive
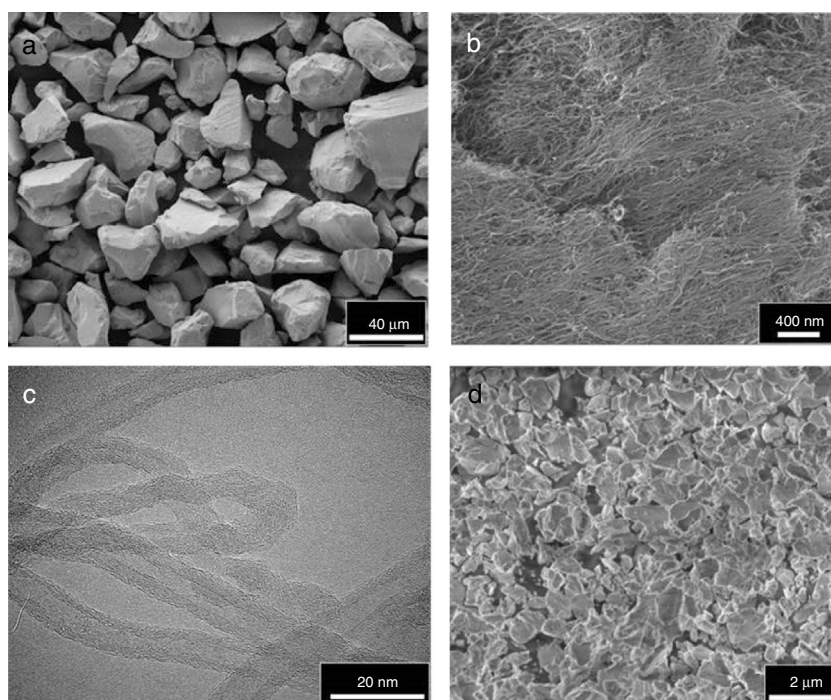

Fig. 1 – Morphology of the starting materials and powders. (a) SEM image of YSZ as received (SE, MAG 500× HV 5 kV), (b) SEM image of MWCNT as received (SE, MAG 10000× HV 5 kV), (c) TEM image of MWCNT as received (at 200 kV) and (d) SEM image milled YSZ after 5 h (SE, MAG 5000× HV 5 kV).
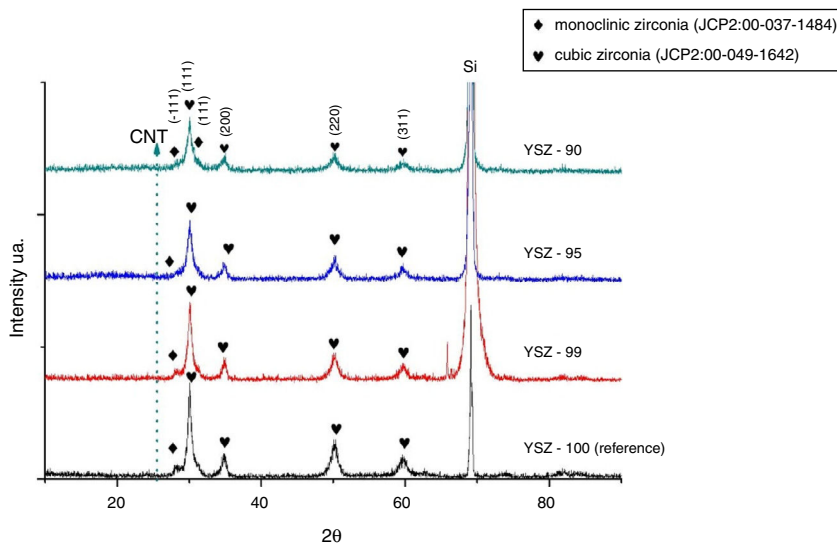
Fig. 2 – XRD patterns of YSZ reference and YSZ/MWCNT powders.

method to investigate the atomic bonding properties and the microstructure. Renishaw 1000 B micro-Raman spectrometer attached to a Leica DM/LM microscope was used to examine Raman spectroscopy at room temperature in the wavenumber range of 150–3500 cm^{-1} with 488 nm laser excitation. The spectral resolution of the system is 2.5 cm^{-1} and the diameter of the excitation spot is 1 μm.

Results and discussion

The YSZ based powder mixtures with various MWCNT additives (1, 5 and 10 wt.%) were prepared by attritor milling (Fig. 1 and Table 1). The result of the phase examination of the reference YSZ and milled powder mixtures is shown in Fig. 2. The milled powders were consisted mainly of cubic zirconia (JCP2:00-049-1642) and minor monoclinic zirconia (JCP2:00-037-1484) phases (Fig. 2). The cubic zirconia is indicated by the main lines appeared at 2θ of 30.24°, 34.88°, 50.17° and 59.69°. While, the minor monoclinic phase was observed at 2θ of 28.36° and 31.12°.As for first observation, the milling process did not resulted in phase transformation only grain decrease occured. YSZ reference base material exhibited well dispersed particles with sharp and irregular shape (Fig. 1). The morphological study of MWCNT demonstrated their agglomerated bundle structure. On the other hand, the addition of MWCNTs to zirconia matrix introduced a significant change in the surface topology and the distribution of the zirconia grains, leading to various forms and shapes compared to the base material (Fig. 3).

The EDS elemental analysis illustrated the features of MWCNTs distribution in zirconia matrix (Fig. 4). This study confirmed that the MWCNTs formed agglomerations with increasing tendency with MWCNTs addition increase (YSZ-99 → YSZ-95 → YSZ-90). The MWCNTs agglomerations (C-red, Fig. 4) were surrounded by ultrafine rounded zirconium

(Zr-blue). Structural investigations of zirconia powder before and after milling process were carried out by TEM (Fig. 5). The TEM investigation demonstrated the decrease of YSZ particle size in average 50 μm to 400 nm.

Structural observations of the mixed powders YSZ-99, YSZ-95, YSZ-90 are shown in Fig. 6. This result shows that the small zirconia grains (<100 nm) and particles (>200 nm) are embedded into MWCNTs agglomerations and networks. The agglomeration, the damage or the defect of MWCNTs has been reported as a big issue responsible of a significant lack in the reinforcement of ceramic composites with MWCNT. From the point of MWCNTs structure the non-destructive milling process was confirmed by HRTEM study. The MWCNTs appeared as a fine fibres forming several agglomerations with an approximate length of 2.5 μm. Each fibre consisted of an average inner diameter 3.8 nm, an average outer diameter 9.13 nm and a number of layers variated from 7 to 9 (Fig. 6b). These results are in accordance with the study performed by Melka et al. [22]. They confirmed the refinement of the grain sizes up to 2 wt.% of MWCNT used for powder mixture processing [22]. Indeed, when the agglomeration of MWCNT occurs, the real amount of MWCNTs located in the grain boundaries is decreasing. Therefore, the agglomerated CNTs introduce heterogeneity and decrease the efficiency of the composite [23–25].

Scanning Raman spectroscopy measurements were performed to confirm the presence of MWCNT in the powder mixtures and determine structural changes caused by the milling process. Four typical Raman spectra are shown in the 150–3500 cm^{-1} wavenumber region, which were measured on powder mixtures with different MWCNT content (Fig. 7). In case of pure YSZ (reference, YSZ-100, black line) scattering peaks at 189, 268, 341, 380, 483, 633 cm^{-1} related to yttria stabilized zirconia which are in accordance with literature works [26,27]. Characteristic Raman peaks of YSZ are less intensive or completely absent in case of YSZ/MWCNTs powders (YSZ-99, YSZ-95, YSZ-90) in the 100 to 700 cm^{-1} wavenumber
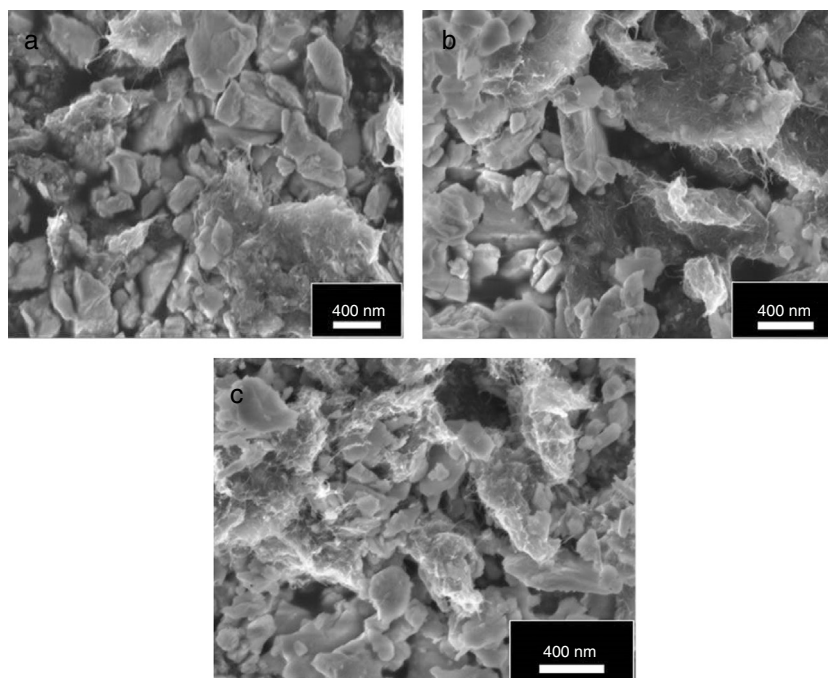
Fig. 3 – SEM images of milled powders. (a) YSZ/1 wt.% MWCNT, (b) YSZ/5 wt.% MWCNT and c) YSZ/10 wt.% MWCNT (SE, MAG 5000× HV 5 kV).
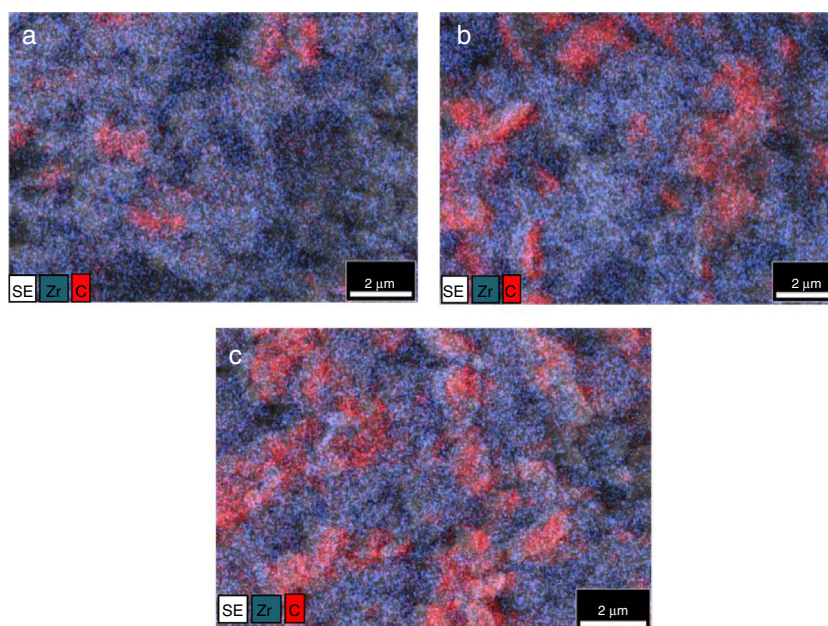

Fig. 4 – EDS mapping showing the dispersion of MWCNTs in YSZ. (a) YSZ/1 wt.% MWCNT, (b) YSZ/5 wt.% MWCNT and (c) YSZ/10 wt.% MWCNT. Colours: C-red and Zr-blue.

region. Additional strong peaks have been observed around 1590 cm^{-1} (G band) and 1355 cm^{-1} (D band), which are related to the MWCNT [28]. The G band is related to the stretching vibration of the sp^2 C–C bonds, while the D band is associated with the presence of structural defects in the MWCNT. Raman spectra also exhibited a wide band at higher wavenumbers,

the so called 2D band, which appears at 2687, 2684 and 2690 cm^{-1} for 1, 5, 10 wt.% MCWNT content, respectively. The 2D band feature originates in a two-phonon, second-order Raman scattering process in carbon nanotubes [29]. The intensity ratio of D and G band (I_D/I_G) has been widely used to investigate the structural purity (structural defects and
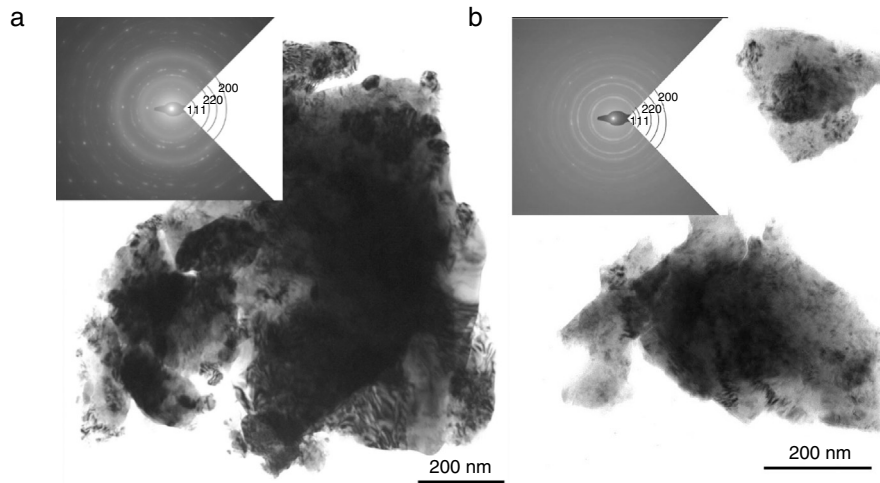
Fig. 5 – TEM images of YSZ with SAED diffraction in insert. (a) Reference before milling and (b) reference after milling. The SAED confirmed the cubic zirconia (111, 220, 200) in both cases.
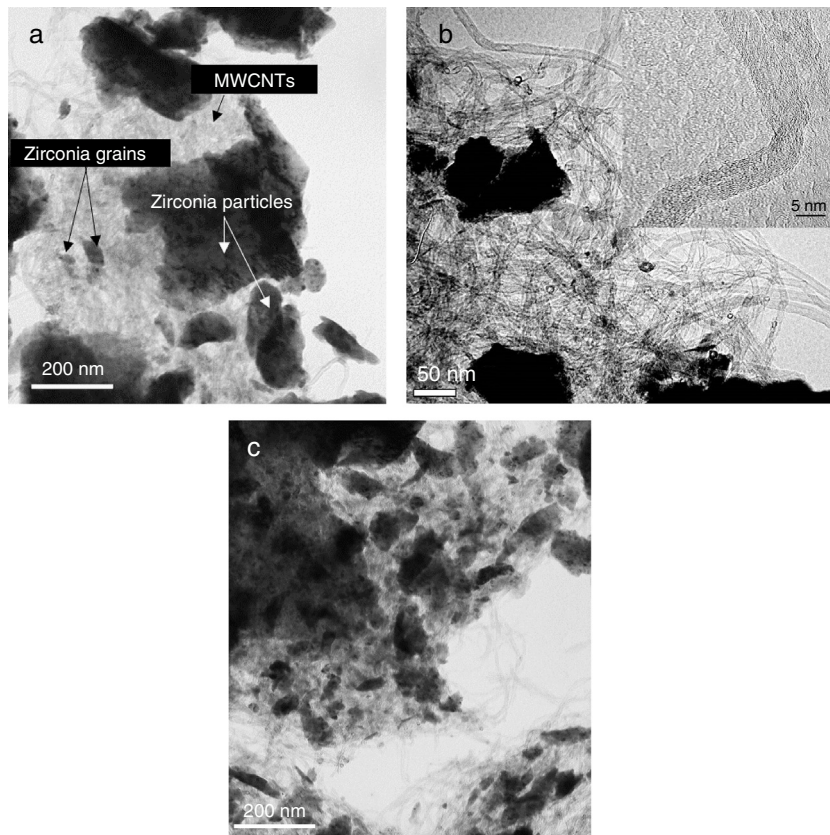

Fig. 6 – TEM images of YSZ/MWCNTs. (a) YSZ/1 wt.% MWCNT, (b) YSZ/5 wt.% MWCNT with detail of MWCNT in insert and (c) YSZ/10 wt.% MWCNT.

disordering) of MWCNTs or the presence of agglomerations [30,31], hence the intensity of D band is defect dependent. In principle, the larger the number of defects, the higher the D band intensity. Peak positions and intensity of distinct scattering bands were determined by Lorentzian fitting of Raman spectra shown in Fig. 7. Although such procedure has some uncertainty because of the number of free parameters,

it can provide additional information about the YSZ/MWCNTs powders. We found that the I_D/I_G ratio is 0.6 for YSZ-99, 0.8 for YSZ-95 and 0.7 for YSZ-90, which values are in good accordance with previous morphological observations showing the presence of structural defects and agglomerations in the YSZ/MWCNTs powders as a result of intensive milling. Among the powder mixtures, YSZ-95 contains more structural
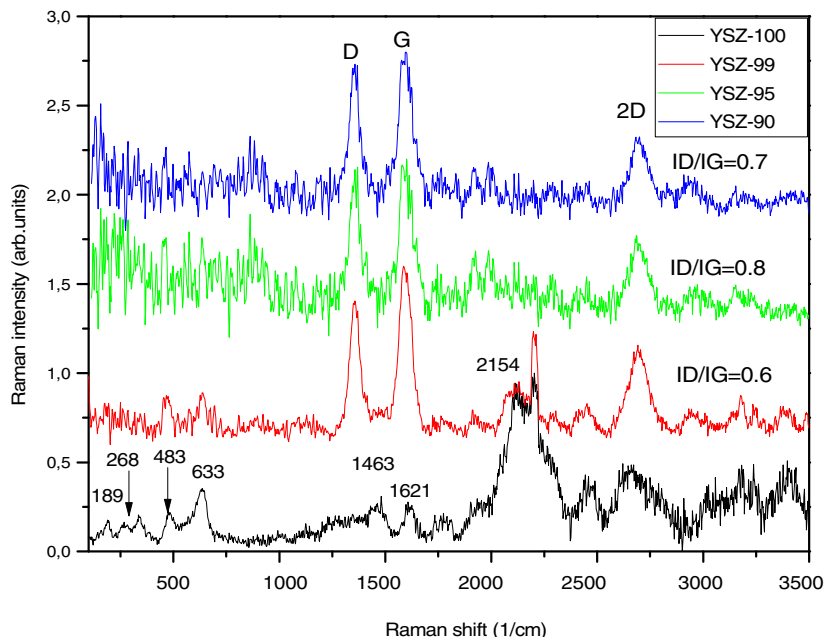
Fig. 7 – Raman spectra using a laser excitation wavelength at 488 nm for reference and YSZ/MWCNTs.

defects compared to the others according to its highest I_D/I_G ratio (0.8).

Conclusion

The aim of our study was the development of YSZ/MWCNTs as nickel free SOFC material. This work showed the main results of first preparation step; milling and homogenization. The influence of MWCNT addition and milling process on structure and design of composites were studied. ZrO_2 – 8 mol.% Y_2O_3 (YSZ) powders were mixed with 1, 5 and 10 wt.% MWCNTs and milled by high attrition milling at 4000 rpm in ethanol for 5 h. The structural and morphological investigations of as-received zirconia powder consisted of the particles with sharp and irregular shape. In fact, the effect of milling on the as received zirconia resulted in a considerable decrease for particle size without phase transformation of YSZ particles. The phase analysis proved the existence of two phases; cubic zirconia as a main phase and a small fraction of monoclinic zirconia as a minor phase. The particle size showed a refinement from an average of 50 μm to 400 nm. However, no significant damage or structural changes affected MWCNTs after milling were observed. The MWCNTs were observed as a fine fibres forming several agglomerations, networks with approximate length 2.5 μm, each fibre consisted of an average diameter 3.8 nm, an average outer diameter 9.13 nm. The number of carbon layers varied from 7 to 9. Raman spectroscopy results showed the presence of the G and D bands for all powder mixtures at peak positions of ∼1590 and ∼1355 cm^{-1} respectively. These bands confirmed the structural integrity of MWCNT after the milling process.

The novel results are follows:

- milling process did not result in phase transformation of YSZ only grain decrease;

- the addition of MWCNTs to zirconia matrix introduced a significant change in the surface topology and the distribution of the zirconia grains;
- from the point of MWCNTs structure, non-destructive milling process was confirmed by HRTEM study;
- the structural integrity of MWCNTs after the milling process was confirmed by Raman measurements too.

Acknowledgement

REFERENCES

[1] N.P. Padture, Multifunctional composites of ceramics and single-walled carbon nanotubes, Adv. Mater. 21 (2009) 1767–1770.

[2] O. Tatsuki, S. Mrityunjay, Engineered Ceramics: Current Status and Future Prospects, 292, 1st ed., John Willey and Sons, Hoboken, NJ, 2016, pp. 291–331, 978-1-119-10040-9.

[3] C.S. Spiegel, Designing & building fuel cells, 42, 1st ed., McGraw-Hill Education: Two penn plaza, New York, 2007, pp. 35–51, 978-0071489775.

[4] E.D. Wachsman, K.T. Lee, Lowering the temperature of solid oxide fuel cells, Science 334 (2011) 935–939.

[5] N. Laosiripojana, S. Assabumrungrat, Catalytic steam reforming of methane, methanol, and ethanol over Ni/YSZ: the possible use of these fuels in internal reforming SOFC, J. Power Sources 163 (2007) 943–951.

[6] T.A. Kamel Halouani, Analytical modeling of polarizations in a solid oxide fuel cell using biomass syngas product as fuel, Appl. Therm. Eng. 27 (2007) 731–737.

[7] A. Alaswad, A. Palumbo, M. Dassisti, A.G. Olabi, Fuel Cell Technologies, Applications, and State of the Art. A Reference Guide. Reference Module in Materials Science and Materials Engineering, 2016, http://dx.doi.org/10.1016/B978-0-12-803581-8.04009-1.

[8] G. Cacciola, V. Antonucci, S. Freni, Technology up date and new strategies on fuel cells, J. Power Sources 100 (2001) 67–79.

[9] L. Mingfei, D. Dehua, P. Ranran, G. Jianfeng, D. Juan, L. Xingqin, M. Guangyao, YSZ-based SOFC with modified electrode/electrolyte interfaces for operating at temperature lower than 650°C, J. Power Sources 180 (2008) 215–220.

[10] O. Tatsuki, S. Mrityunjay, Engineered Ceramics: Current status and Future Prospects, 422, 1st ed., John Willey and Sons, Hoboken, NJ, 2016, pp. 415–425, 978-1-119-10040-9.

[11] Y.L. Lium, A. Hagen, R. Barfod, M. Chen, H.J. Wang, F.W. Poulsen, P.V. Hendriksen, Microstructural studies on degradation of interface between LSM–YSZ cathode and YSZ electrolyte in SOFCs, Solid State Ion 180 (2009) 1298–1304.

[12] T. Priyatham, B. Ranjit, Synthesis and characterization of nanocrystalline Ni–YSZ cermet anode for SOFC, Mater. Charact. 61 (2010) 54–58.

[13] S.P. Jiang, Y.Y. Duan, J.G. Love, Fabrication of high-performance Ni/Y_2O_3–ZrO_2 cermet anodes of solid oxide fuel cells by ion impregnation, J. Electrochem. Soc. 149 (2002) 1175–1186.

[14] Z. Cheng, M. Liu, Characterization of sulfur poisoning of Ni–YSZ anodes for solid oxide fuel cells using in situ Raman micro spectroscopy, Solid State Ion 178 (2007) 925–935.

[15] K.M. Shirjeel, B.L. Seung, H.S. Rak, W.L. Jong, T.L. Hyosung, S.J. Parka, Fundamental mechanisms involved in the degradation of nickel–yttria stabilized zirconia (Ni–YSZ) anode during solid oxide fuel cells operation: a review, Ceram. Int. 42 (2016) 35–48.

[16] M. Tanhaei, M. Mozammel, Yttria-stabilized zirconia thin film electrolyte deposited by EB-PVD on porous anode support for SOFC applications, Ceram. Int. 43 (3) (2017) 3035–3042.

[17] B. Usmani, V. Vijay, R. Chhibber, A. Dixit, Optimization of sputtered zirconium thin films as an infrared reflector for use in spectrally-selective solar absorbers, Thin Solid Films 627 (2017) 17–25.

[18] R. Amirante, E. Cassone, E. Distaso, P. Tamburrano, Overview on recent developments in energy storage: mechanical, electrochemical and hydrogen technologies, Energy Conver. Manag. 132 (2017) 372–387.

[19] A.P.P. Alves, R. Koizumi, A. Samanta, L.D. Machado, A. Singh, D.S. Galvao, G.G. Silva, Ch.S. Tiwaryand, P.M. Ajayan, One-step electrodeposited 3D-ternary composite of zirconia nanoparticles rGO and poly pyrrole with enhanced supercapacitor performance, Nano Energy 31 (2017) 225–232.

[20] S.M. El-Eskandarany, E. Shaban, H. Al-Matrouk, M. Behbehani, A. Alkandary, F. Aldakheel, A. Naser, S.A. Ahmed, Structure, morphology and hydrogen storage kinetics of nanocomposite MgH_2/10 wt% $ZrNi_5$ powders, Mater. Today Energy 3 (2017) 60–71.

[21] S. Kumar, et al., Surface modification of MgH_2 by $ZrCl_4$ to tailor the reversible hydrogen storage performance, Int. J. Hydrogen Energy (2017), http://dx.doi.org/10.1016/j.ijhydene.2017.01.193.

[22] L. Melk, et al., Nanoindentation and fracture toughness of nanostructured zirconia/multi-walled carbon nanotube composites, Ceram. Int. (2014), http://dx.doi.org/10.1016/j.ceramint.2014.10.060.

[23] A. Gallardo-Lopez, A. Morales-Rodríguez, J. Vega-Padillo, R. Poyatob, A. Munoz, A. Domínguez-Rodrígueza, Enhanced carbon nanotube dispersion in 3YTZP/SWNTs composites and its effect on room temperature mechanical and electrical properties, J. Alloys Compd. 682 (2016) 70–79.

[24] A. Duszová, J. Dusza, K. Tomsek, J. Morgiel, B. Gurdial, J. Kuebler, Zirconia/carbon nanofiber composite, Scr. Mater. 58 (2008) 520–523.

[25] A. Duszová, J. Dusza, K. Tomsek, J. Morgiel, B. Gurdial, J. Kuebler, Microstructure and properties of carbon nanotube/zirconia composite, J. Eur. Ceram. Soc. 28 (2008) 1023–1102.

[26] A. Ghosh, A.K. Suri, M. Pandey, S. Thomas, T.R. Rama Mohan, B.T. Rao, Nanocrystalline zirconia-yttria system – a Raman study, Mater. Lett. 60 (2006) 1170–1173.

[27] J. Cai, Y.S. Raptis, E. Anastassakis, Stabilized cubic zirconia: a Raman study under uniaxial stress, Appl. Phys. Lett. 62 (1993) 2781.

[28] L. Bokobza, J. Zhan, Raman spectroscopic characterization of multiwall carbon nanotubes and of composites. *eXPRESS Poly*, Letters 6 (2012) 601–608.

[29] M.S. Dresselhaus, et al., Raman spectroscopy of carbon nanotubes, Phys. Rep. 409 (2005) 47–99.

[30] E. Bódis, I. Cora, C. Balázsi, P. Németh, Z. Károly, S. Klébert, P. Fazekasa, A.M. Keszlera, J. Szépvölgyia, Spark plasma sintering of graphene reinforced silicon carbide ceramics, Ceram. Int. 43 (2017) 9005–9011.

[31] E.F. Antunesa, A.O. Lobo, E.J. Corata, V.J. Trava-Airoldia, A.A. Martin, C. Verı simo, Comparative study of first- and second-order Raman spectra of MWCNT at visible and infrared laser excitation, Carbon 44 (2006) 2202–2211.